Proceedings of the 1993 IEEE/RSJ International Conference on Intelligent Robots and Systems Yokohama, Japan July 26-30, 1993

Simulated and Experimental Results of Dual Resolution Sensor Based Planning for Hyper-redundant Manipulators

N. Takanashi* H. Choset† and J. W. Burdick‡

Dept. of Mechanical Engineering, Mail Code 104-44, CALTECH, Pasadena, CA 91125

ABSTRACT: This paper presents a dual-resolution *local* sensor based planning method for hyper-redundant robot mechanisms. Two classes of sensor feedback control methods, working at different sampling rates and different spatial resolutions, are considered: *full shape modification* (FSM), and *partial shape modification* (PSM). FSM and PSM cooperate to utilize a mechanism's hyper-redundancy to enable both local obstacle avoidance and end-effector placement in real-time. These methods have been implemented on a thirty degree of freedom hyper-redundant manipulator which has eleven ultrasonic distance measurement sensors and twenty infrared proximity sensors. The implementation of these algorithms in a dual CPU real-time control computer, an innovative sensor bus architecture, and a novel graphical control interface are described. Experimental results obtained using this test bed show the efficacy of the proposed method.

1. Introduction

This paper presents preliminary experimental results in the area of *local sensor based planning* for hyper-redundant robot manipulators. Recall from [ChB90b] that a "hyper-redundant" manipulator is a kinematically redundant manipulator in which the degree of redundancy is very large or infinite. Such robots are analogous in morphology to tentacles or snakes. "Sensor based planning" incorporates sensory information into some stage of a robotic motion planning, whether it be navigation, locomotion, grasping, etc. Based on information gathered from sensors, "local sensor based planning" modifies the robot's plan over a span which is short in time or distance.

Due to their high degree of articulation, hyper-redundant robots are potentially superior for operations in highly constrained and unusual environments encountered in applications such as inspection of nuclear reactor cores, chemical sampling of buried toxic waste, and medical endoscopy. Hyper-redundant robots can also be used as tentacle-like grasping devices for capturing and manipulating floating satellites [ChB90c] or to enable complex "whole arm manipulation." Mobile hyper-redundant robots also offer novel means for locomotion [ChB91a, ChB93a, ChB93b, ChB93c] in complex environments.

The aforementioned applications are characterized by environments which are difficult to precisely model and which are time varying. Thus, local sensor-based motion planning schemes are vital to the realistic deployment of hyper-redundant robots in these applications. While hyper-redundant robots have many advantages for the above described applications, they have one disadvantage. Since hyper-redundant manipulators have a large number of joints or actuators, small joint displacement errors can accumulate to reasonably large errors in the position of the tip relative to the base. Thus, the effective accuracy of hyper-redundant robots could be improved by distributing sensors along their length and employing sensor based planning schemes.

Thus, local sensor based planning can be used to: (1) account for spatial uncertainty or inaccuracies in the world model used by a "global" planner to construct a robot plan; (2) increase the effective accuracy of a hyper-redundant robot mechanism; and (3) locally adapt to rapid environmental variations, such as moving obstacles, that can not be easily or rapidly handled by a global planner.

In this paper, the local sensor based planning algorithms of hyper-redundant manipulators are based on the hyper-redundant kinematic analysis found in [ChB90b, ChB91a, ChB92a, ChB92c, Ch]. More importantly, we demonstrate these algorithms on an actual 30 degree-of-freedom hyper-redundant robot system. A more detailed account of this mechanism and its capabilities can be found in [ChB92b]. These experiments demonstrate that local sensor based planning is not only useful, but also implementable in real time with very reasonable computing power and simple sensors.

Robotic motion planning has been an important area of research. Since the introduction of configuration space methods [LoWes], several other theories have been published, some of which are summarized in [Sh,Latombe]. However, these methods assume that complete knowledge of the environment is available prior to planning. More recently, methods have been developed which assume the robot explores the environment to gather information for the planning process [CaLi]. These approaches assume that the sensors provide perfect information about the environment. There has been little work devoted explicitly to motion planning for robot snakes. One approach is based on the construction of *tunnels* through the obstacle field, through which the manipulator "slithers" [ChB90a, Ch]. In another work, sensor based planning for highly redundant robots is based on a *tactrix* [ReLu]. However, this work assumes that there are perfect sensors on the robot; nor has it been implemented on a real robot. Hirose [HiU] implemented an "active cord" mechanism, which used tactile sensors to guide its motion. Our work presents preliminary strategies for local sensor based planning, which are implementable in real time, can employ a variety of sensors, and exploit the benefits of hyper-redundancy.

The structure of this paper is as follows. Section 2 reviews the basic framework of hyper-redundant manipulator kinematics which is based on "backbone curves." The backbone curve and its deformation is the basis for the algorithms of Section 3. We primarily consider algorithms for planar mechanisms, as the experimental verification of these ideas was performed on a planar robot. Many of these algorithms can be extended to the spatial case. Section 4 describes the experimental setup, while Section 5 described the actual results of these experiments.

2. Background

This section reviews a hyper-redundant robot kinematic analysis framework that forms the basis of this work. Recall from [ChB90b] that we assume that (regardless of mechanical implementation) the important macroscopic features of a hyper-redundant robot can be captured by a *backbone curve*. A backbone curve parametrization and an associated set of reference frames which evolve along the curve are collectively called the *backbone reference set*. In this paradigm, inverse kinematics and task planning reduces to

* Visiting Researcher from NEC Corporation

† Graduate Student

‡ Assistant Professor

0-7803-0823-9/93/$3.00 (C) 1993 IEEE

the determination of the proper time varying behavior of the backbone reference set [ChB90b]. Similarly, local sensor based planning is equivalent in this approach to modification of the backbone curve shape in order to accommodate impinging obstacles.

In [ChB92c],many techniques are introduced for parametrizing the backbone curve. In this paper, we will assume that the Cartesian position of points on a backbone curve can be parametrized in the form:

$$\vec{x}(s,t) = \int_0^s l(\sigma,t)\, \vec{u}(\sigma,t) d\sigma \tag{2.1}$$

where $s \in [0,1]$ is a parameter measuring distance along the backbone curve at time t. The *backbone curve base* is the point $s = 0$. $\vec{x}(s,t)$ is a vector from the backbone curve base to point s. By convention, $\vec{x}(0,t) = 0$. $\vec{u}(s,t)$ is the unit tangent vector to the curve at s. $l(s,t)$ is the length of the curve tangent and assumes the general form:

$$l(s,t) = 1 + \epsilon(s,t) > 0. \tag{2.2}$$

$\epsilon(s,t)$ is the *local extensibility* of the manipulator, which expresses how the backbone curve locally expands or contracts relative to a fixed reference state. The parametrization of Eq. (2.1) has the following interpretation. The backbone curve is "grown" from the base by propagating the curve forward along the tangent vector, which is varying its direction according to $\vec{u}(s,t)$ and varying its magnitude (or 'growth-rate') according to $l(s,t)$.

Our experiments have been performed on a device with planar geometry. In the planar case, the backbone curve is the locus of points:

$$\vec{x}(s,t) = [x_1(s,t),\ x_2(s,t)]^T$$

where

$$x_1(s,t) = \int_0^s l(\sigma,t) \sin\theta(\sigma,t) d\sigma \tag{2.3}$$

$$x_2(s,t) = \int_0^s l(\sigma,t) \cos\theta(\sigma,t) d\sigma. \tag{2.4}$$

$\theta(s,t)$ is the angle, measured clockwise, which the tangent to the curve at s makes with the x_2-axis at time t. By convention (2.4), $\theta(0) = 0$, and $x_1(0) = x_2(0) = 0$. By comparing equations (2.1) with equations (2.3) and (2.4), it easy to see that $\vec{u}(s,t) = [\sin\theta(s,t),\ \cos\theta(s,t)]^T$ in the planar case. $l(s)$ and $\theta(s)$ are termed "shape functions," as they control they shape of the backbone curve through the forward kinematic relations (2.3) and (2.4).

Within the context of this modeling technique, the inverse kinematic problem, or "hyper-redundancy resolution" problem, reduces to the determination of the time varying behavior of backbone curve shape functions that satisfies task requirements. Different hyper-redundancy resolution techniques can be found in [ChB90a, ChB91a, ChB92a, ChB92c, Ch]. In one approach, which is relevant to the algorithms of Section 3, the backbone curve shape functions are restricted to a "modal form"

$$\theta(s,t) = \sum_{i=1}^{N_\theta} a_i(t)\ \Phi_i(s) \qquad l(s,t) = \sum_{i=N_\theta+1}^{N_l} a_i(t)\ \Phi_i(s) \tag{2.5}$$

where $\Phi_i(s)$ is a "mode function," and $a_i(t)$ is the associated "modal participation factor." $N = N_\theta + N_l$ is the total number of modes, which must equal or exceeds the number of task constraints. Hyper-redundancy is resolved in the modal approach by constraining the backbone curve to N effective DOF. The $\{\Phi_i\}$ are predetermined functions chosen by the programmer, and can often be selected to incorporate physical characteristics of the task [Ch]. Thus, the backbone curve geometry becomes solely a function of the $\{a_i\}$. The inverse kinematics problem reduces to finding the $\{a_i\}$ which satisfy task constraints.

In [ChB91a, ChB92c], closed form solutions are given for several choices of mode functions. However, this method can also be used when closed form modal solutions do not exist. This computational scheme, which is analogous to the resolved rate trajectory planning method, is based on a *modal Jacobian*, $\mathcal{J}$, which relates infinitesimal changes in $\vec{a}$ to infinitesimal changes in the end-effector position:

$$\delta\vec{x}_{ee} = \mathcal{J}\delta\vec{a} \tag{2.6}$$

where

$$\mathcal{J}_{ik} = \frac{\partial x_i}{\partial a_k} \tag{2.7}.$$

For a given initial set of modal participation factors, $\vec{a}_0$, Eq. (2.6) can be solved to determine the incremental changes in $\vec{a}$ to follow incremental changes in the desired end-effector trajectory:

$$\delta\vec{a} = \mathcal{J}^{-1}(\vec{a})\delta\vec{x}_{ee}. \tag{2.8}$$

By $\mathcal{J}^{-1}$ we imply a generalized inverse if $\mathcal{J}$ is non-square. These incremental changes can be used in an iterative procedure to modify the participation factors, i.e, $\vec{a}(t+\delta t) = \vec{a}(t)+\delta\vec{a}$, starting with $\vec{a}(0) = \vec{a}_0$.

A continuous backbone curve inverse kinematic solution is used to determine the actuator displacements of a continuous morphology robot such as one constructed from pneumatic actuator bundles. For discretely segmented morphologies, such as the prototype described in this paper in Section 4, the continuous curve solution can be used, via a "fitting" process, to compute the actuator displacements which cause the manipulator to exactly assume or closely approximate the continuous backbone curve model. The fitting techniques which are used in subsequent examples are reviewed in [ChB91a, ChB92c].

3. Local Sensor Based Planning Algorithms

In Local Sensor-Based Planning (LSBP), we assume that a backbone curve is somehow determined by a high level global planning process. The backbone curve shape is then modified in response to sensory information. LSBP does not use a model of the environment, and is intended for rapid response to environment changes.

3.1. Dual-resolution local sensor based planning method

We suggest a dual-resolution approach to LSBP based on: (1) full-shape modification, or FSM; and (2) partial shape modification, or PSM. FSM and PSM work at different sampling rates and at different spatial resolutions. Together, they cooperate to effectively utilize hyper-redundancy in a way which enables rapid local response in real time to the environment while also satisfying more global task constraints, such as end-effector positioning. Fig.1 shows the relation between FSM, PSM and the actual robot.

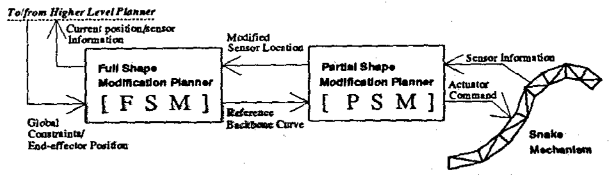
To/from Higher Level Planner
Current position/sensor Information
Modified Sensor Location
Sensor Information
Full Shape Modification Planner [F S M]
Partial Shape Modification Planner [P S M]
Actuator Command
Reference Backbone Curve
Global Constraints/ End-effector Position
Snake Mechanism

Figure 1: Dual-resolution local sensor based planning method

The FSM determines the entire backbone curve shape using position and task constraints from a high level planner and information about nearby obstacles which is derived from sensor data.

The generated backbone curve shape is passed to the PSM as a reference shape. In response to changes detected by sensors, the PSM stage modifies the reference backbone curve shape in a local neighborhood around the sensor. Finally, actuator commands are generated to realize the modified shape. The PSM sends the modification result to FSM. This information is used in the next FSM planning cycle.

The FSM planner is expected to be more computationally intensive than the PSM. First, the FSM stage must satisfy some global task constraints, such as fixed end-point positioning. In addition, the FSM planner may use sensors, such as vision or ultrasound, which require non-trivial computation. Thus, the cycle rate of FSM is slower than the mechanism servo rate, and perhaps not fast enough to respond to rapid changes. Conversely, PSM algorithms, which only consider localized sensor information, can be quite simple, and thus computationally efficient. Further, since the PSM response is localized, the PSM computation can be performed in parallel by processors distributed along the mechanism. Finally, the PSM stage can use rapid response simple sensors or simply processed data from more complex sensors. This enables the PSM stage to be computed at a rapid rate—often at the mechanism servo rate. Thus, the FSM/PSM decomposition takes maximum advantage of practical considerations in algorithm computation and sensor processing.

While the PSM enables rapid local modification, it has limitations. For example, when the actuators in the vicinity of a particular sensor are unable to carry out local modifications because they are near their limits (or a local mechanism singularity), the PSM detects this condition, and informs the FSM to modify the entire backbone curve. This is an important feature of our approach–an explicit indication when a particular strategy is required.

3.2. Sensor Models

The algorithms described below use a very simple sensor model. We assume that the sensors are rigidly attached to the backbone curve at a fixed point. That is, they move with the backbone curve, and their orientation is a function of the backbone curve tangent at the point of attachment. The sensors are assumed to measure, along a fixed direction termed the *sensor measurement axis*, the distance to a nearby obstacle. The sensor measurement axis is a function of the sensor and the backbone curve geometry (See Fig. 2). Our sensors *do not* measure the distance to the point on the obstacle which is nearest to the backbone curve. Rather, they measure the distance which would actually be computed by realistic sensors. This simple model is representative of the infrared and ultrasonic sensors discussed in Section 4. In addition, there is often some directional ambiguity due to the finite width of a typical sensor's beam pattern. We assume that the sensor measurement axis is the centerline of the beam pattern. The distance measurement returned by the sensor is the nearest point of the obstacle lying within beam pattern cone. Since it is impossible to resolve the angular ambiguity, we assume that nearest point of the obstacle lies along the beam pattern centerline.

3.3. Full-shape modification (FSM) control method

There are a variety of techniques for implementing an FSM planner. Described below is one approach based on the modal inverse kinematic method of [ChB92c, Ch]. The goal is to determine how to vary the modal participation factors, using both task and sensor data, so as to satisfy both end point positioning and obstacle avoidance.

Let the manipulator end point velocity vector be denoted $\dot{\vec{x}}$. For a manipulator constrained to a set of modes, $\{\Phi_i\}$, $\dot{\vec{x}}$ is related to

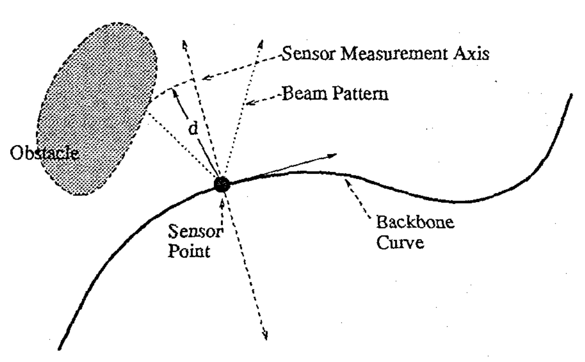

Figure 2: Simplified Distance Measurement Sensor Model

the time derivative of modal participation factor vector $\vec{a}$ by:

$$\dot{\vec{x}} = \mathcal{J}\dot{\vec{a}}. \quad (3.3.1)$$

If $m = dim(\vec{x})$, $\mathcal{J}$ is an $m \times N$ matrix, where N is the number of modes. N is typically much less than the number of actual mechanical degrees of freedom. When $N = m$, the positioning control equation is non-redundant in modal participation factor space, even though a hyper-redundant manipulator is being controlled.

Obstacle avoidance and end-effector placement is achieved by adding r additional mode functions to the minimal mode function set, where r is greater than or equal to the number of extra constraints imposed by obstacle avoidance. However, if r is not large enough, the algorithm below will try to satisfy constraints in a least squares sense.

In this method, a modal participation factor null-space projection improvement scheme based on the modal Jacobian pseudo inverse [Liegeois] is adopted. Let $\mathcal{J}^{\dagger}$ denote the Moore-Penrose pseudo inverse [Pe] of the $m\times(m+r)$ modal Jacobian matrix. The general solution to Eq.(3.3.1) for given $\dot{\vec{x}}$ is [Gr]:

$$\dot{\vec{a}} = \mathcal{J}^{\dagger}\dot{\vec{x}} + (I - \mathcal{J}^{\dagger}\mathcal{J})\vec{z} \quad (3.3.2)$$

where, I is an $(m+r)\times(m+r)$ identity matrix and $\vec{z}$ is an arbitrary vector in $\dot{\vec{a}}$-space. We now consider how to compute $\vec{z}$ based on sensor data and modally constrained backbone curve kinematics.

Yoshikawa [Yo] has implemented a model based obstacle avoidance scheme by selecting $\vec{z}$ as a collision-free joint space vector. Maciejewski[MaKl] has proposed a real time scheme by introducing an obstacle avoidance vector to determine $\vec{z}$. Nakamura [Nak] has developed task priority redundancy resolution methods when there are multiple objectives. Our method is a variant of these approaches, but in the modal participation factor space.

In this method, an "obstacle point", $\vec{O}$, is a point on the backbone curve which has to avoid nearby obstacles. In practice, we choose $\vec{O}$ to be the location of a sensor along the backbone curve. The backbone curve distance measure to point $\vec{O}$ is denoted by s_O.

The differential kinematics of the end point and obstacle point are:

$$\mathcal{J}_e\dot{\vec{a}} = \dot{\vec{x}} \quad (3.3.3)$$

$$\mathcal{J}_O\dot{\vec{a}} = \dot{\vec{O}} \quad (3.3.4)$$

where $\mathcal{J}_e$ is the end-point modal Jacobian and $\mathcal{J}_O$ is the modal Jacobian associated with the "obstacle-point." $\mathcal{J}_O$ is a matrix of size $o \times (m + r)$, where o is the dimension of the obstacle avoidance task. $\dot{\vec{O}}$ is the "obstacle-point velocity vector," which is the direction the obstacle point should move to avoid the obstacle. As suggested by Section 3.2, this direction is collinear with sensor measurement axis and its magnitude is a function of the distance to the obstacle.

Substituting Eq.(3.3.2) into Eq.(3.3.4), yields

$$\mathcal{J}_O \mathcal{J}_e^{\dagger} \dot{\vec{x}} + \mathcal{J}_O (I - \mathcal{J}_e^{\dagger} \mathcal{J}_e) \vec{z} = \dot{\vec{O}} \tag{3.3.5}$$

Solving Eq.(3.3.5) for $\vec{z}$ and substituting back into Eq.(3.3.2), the time derivative of the desired modal participation factor vector is:

$$\dot{\vec{a}} = \mathcal{J}_e^{\dagger} \dot{\vec{x}} + [\mathcal{J}_O (I - \mathcal{J}_e^{\dagger} \mathcal{J}_e)]^{\dagger} (\dot{\vec{O}} - \mathcal{J}_O \mathcal{J}_e^{\dagger} \dot{\vec{x}}) \tag{3.3.6}$$

where the matrix equality $B[CB]^{\dagger} = [CB]^{\dagger}$ was used. If $\dot{\vec{x}} = 0$, Eq. (3.3.6) computes the variation in $\vec{a}$ which causes the end-effector to remain fixed while modifying the backbone curve shape, thus moving the obstacle point in the desired direction. If r is not sufficiently large, obstacle avoidance will be satisfied in a least-squares manner. Also this equation easily generalizes to multiple obstacle points, allowing multiple sensors located along the backbone curve. squares sense.

For some complicated time varying obstacle trajectories, the integration of Eq. (3.3.6) may cause the hyper-redundant mechanism to become entangled after many cycles of computation. This problem can be avoided by introducing a "pseudo-spring" which tends to pull the backbone curve back to its original shape when the obstacles are removed. Eq. (3.3.6) is divided into two parts to realize pseudo spring computation. In discrete time units, the modal participation factor control law is described by:

$$\delta\vec{a}_e(t+1) = \delta\vec{a}_e(t) + \mathcal{J}_e^{\dagger} \delta\vec{x} \tag{3.3.7}$$

$$\vec{a}(t+1) = \vec{a}(t) + \delta\vec{a}_e(t+1) + K[\mathcal{J}_O (I - \mathcal{J}_e^{\dagger} \mathcal{J}_e)]^{\dagger} (\dot{\vec{O}} - \mathcal{J}_O \mathcal{J}_e^{\dagger} \delta\vec{x}) \tag{3.3.8}$$

where, $\delta a_e(t)$ is the modal participation factor modification for end-point positioning and K is an $(m + r) \times o$ matrix of "pseudo spring constants." Eq. (3.3.7) updates and holds the modal participation factors to perform end-point positioning. The modal participation factors for positioning are modified by the second term for object avoidance in Eq. (3.3.8). The modified result is used to determine the backbone curve. Since the modification for obstacle avoidance affects the change of modal participation factors at time t through the spring constant K, once the obstacles are gone, the backbone curve returns back to its original shape.

As an example, consider a system with three sensors distributed along the nonextensible planar manipulator backbone curve. In this case, $l(s) = 1 \ \forall s$ and $\theta(s)$ is constrained to the five modes:

$$\begin{aligned}
\Phi_1(s) &= \frac{1}{2\pi} \sin(\frac{2\pi}{L} s) \\
\Phi_2(s) &= \frac{1}{2\pi} \cos(\frac{2\pi}{L} s) \\
\Phi_3(s) &= \frac{1}{L} s \\
\Phi_4(s) &= \frac{1}{6\pi} \cos(\frac{6\pi}{L} s) \\
\Phi_5(s) &= \frac{1}{6\pi} \sin(\frac{6\pi}{L} s)
\end{aligned} \tag{3.3.9}$$

where L is the total length of the mechanism. Practically speaking, the first three functions mainly contribute to the end-effector positioning and orientation, while the other two contribute to obstacle avoidance capability.

The obstacle points in Eq. (3.3.4) correspond to sensor points, which are located at distances $L/4$, $L/2$, $3L/4$ along the backbone curve. The obstacle avoidance vector is selected parallel to the sensor measurement axis. We assume that the sensors are rigidly attached to the mechanism, so that the direction of this vector is configuration dependent. Simulation results are shown in Fig. 4 and Fig. 3. Three obstacles (denoted by circles in figure) are located close to the backbone curve. The end-point location, position and orientation, is specified first. Next, the backbone curve is determined using Eq. (3.3.1). Then the curve is modified using Eq. (3.3.7) and Eq. (3.3.8) based on the simulated sensor information. In both figures, triangles show the sensor-points. The dotted lines show the original curve which is generated by end-point positioning. The solid lines represent the modified curve with obstacle avoidance. Both modified curves avoid the obstacle, while the original curve touches them. This result shows the efficacy of this method to full-shape modification control method.

The difference between Fig.4 and Fig.3 is in one obstacle location. In this task, the required total degree of freedom is nine, three for positioning and six (2×3) for the obstacle-point motion. Although using only five different modal function, this nine degree of freedom task requirement is satisfied. The result shows the least-square nature of this algorithm.

3.4. Partial-shape Modification Control

More than one PSM strategy has been implemented on our testbed. This section describes one PSM planning strategy in which the backbone curve is approximated by a large number, n_d, of discrete endpoints. The sensors are assumed to be rigidly attached at points along the discretized backbone curve. There are typically many approximating segments between adjacent sensor

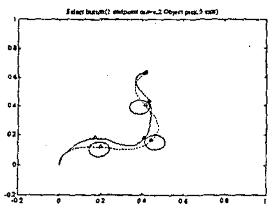
Figure 3: FSM I

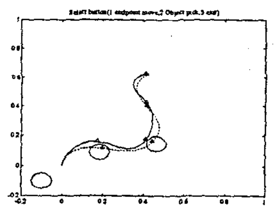
Figure 4: FSM II

attachments. When a sensor detects the presence of an obstacle, the backbone curve shape locally deforms in a region around the sensor. In our simulations and experiments, $n_d \sim 100$, and there were about 10 discrete points between sensor points.

The actual response, a displacement of the approximating points, is determined by a *local sensor response function* (LSRF), which is assumed to be a discrete unimodal function. A unimodal function is one which has one local maximum, the global maximum, over its domain. The response function is "added" to the backbone curve, locally drawing it away from an obstacle. In Figure 5, a triangle LSRF is added to a straight backbone curve, deforming the backbone curve away from an unacceptably close obstacle.

Since the robot only detects the obstacle at a sensor point, the reaction to the obstacle should be greatest at the sensor point, and should monotomically decrease at points away from the sensor point. Therefore, the sensor point is the center of this unimodal function, and is assumed to be farthest away from the obstacle.

The LSRF should also look like the beam pattern of the sensor associated with the sensor point. Typically, beam patterns have a central lobe along the sensor axis, in which the obstacle likely lies.

In the experimental setup, the spatial resolution of the robot's actuators is much lower than the azimuth resolution of the sensors on the robot. Therefore, a simple triangle (or cone) is a sufficient approximation to the main lobe of the beam pattern, and thus, a reasonable choice for a LRSF. Later on, it is shown that a triangle response function leads to a trivial and efficient solution to LSBP for planar hyper-redundant manipulators. So, the example displayed in Figure 5 is a good example of a LSRF.

The half width of the LSRF is slightly larger than the distance between two adjacent sensors on the backbone curve. This way, if two adjacent sensors detect the same obstacle, their cumulative response function is still unimodal.

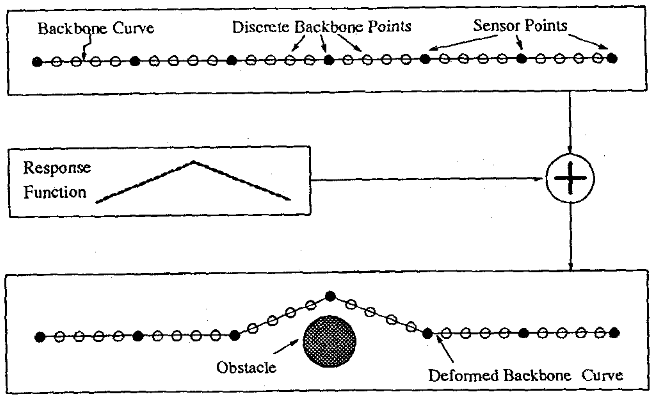

Figure 5: Backbone Curve, Response Function, and Deformed Backbone Curve

In this approximation method, the position of the discrete segment endpoints can be approximated by the discretization of the continuous forward kinematics integral (Eq. (2.1)):

$$\vec{p}(s_i,t) = \sum_{k=0}^{k=i} l(s_k,t)\vec{u}(s_k,t) \tag{3.4.1}$$

$l(s)$ and $\vec{u}(s)$ are continuous shape functions which are specified by the FSM or a global planner. They need not assume a modal form. Also, an endpoint may or may not coincide with a sensor point.

A small differential change in $\vec{p}(s_i)$ is:

$$\delta\vec{p}(s_i,t) = \sum_{k=0}^{k=i} \delta l(s_k,t)\vec{u}(s_k,t) + l(s_k,t)\delta\vec{u}(s_k,t) \tag{3.4.2}$$

where $s_k = \frac{k}{n_d}$, where n_d is the number of discrete points along the back bone curve. $\delta\vec{u}$ is a local change in the backbone curve tangent direction, while $\delta\vec{l}$ represents a local stretch.

The goal of this PSM method is to compute the local perturbations, $\delta\vec{u}$ and $\delta\vec{l}$, which deform the backbone curve away from obstacles. The changes in backbone curve tangent and stretch are determined from $\delta\vec{p}$, which in turn is determined by the LSRFs. The modified backbone curve shape is then used by the fitting algorithms to determine the appropriate actuator displacements.

Assume that at some initial time, the FSM specifies a global backbone curve shape. Thus, $\delta\vec{p} = 0$ initially. For each sensor point along the backbone curve that detects an obstacle within its response envelope, a discrete unimodal LSRF is added to (or subtracted from, depending upon from which direction an obstacle appears to be) δp, the vector which contains the prescribed changes to the backbone curve. Setting $\delta p(s_n,t) = 0$, guarantees that, within the limits of the discretization approximation, the end effector position will not change. Setting $\delta p(s_n,t) = 0$, $\delta p(s_{n-1},t) = 0$, and $\delta\vec{u}(s_n,t) = \vec{0}$ guarantees that the end effector position and orientation will not change. The new backbone curve can be computed after $\delta\vec{u}$ and $\delta\vec{l}$ are determined from (3.4.1).

In the case of a planar backbone curve, (3.4.2) can be written in matrix form:

$$\begin{pmatrix} \delta p_x^1 \\ \delta p_y^1 \\ \delta p_x^2 \\ \delta p_y^2 \\ \vdots \\ \delta p_x^{n-1} \\ \delta p_y^{n-1} \\ \delta p_x^n \\ \delta p_y^n \end{pmatrix} = \begin{pmatrix} l_1 & 0 & 0 & 0 & \dots & 0 & 0 & u_x^1 & 0 & 0 & \dots & 0 \\ 0 & l_1 & 0 & 0 & \dots & 0 & 0 & u_y^1 & 0 & 0 & \dots & 0 \\ l_1 & 0 & l_2 & 0 & \dots & 0 & 0 & u_x^1 & u_x^2 & 0 & \dots & 0 \\ 0 & l_1 & 0 & l_2 & \dots & 0 & 0 & u_x^1 & u_y^2 & 0 & \dots & 0 \\ \vdots & \vdots & \vdots & \vdots & \ddots & \vdots & \vdots & \vdots & \vdots & \vdots & \ddots & \vdots \\ l_1 & 0 & l_2 & 0 & \dots & 0 & 0 & u_x^1 & u_x^2 & u_x^3 & \dots & 0 \\ 0 & l_1 & 0 & l_2 & \dots & 0 & 0 & u_y^1 & u_y^2 & u_y^3 & \dots & 0 \\ l_1 & 0 & l_2 & 0 & \dots & l_n & 0 & u_x^1 & u_x^2 & u_x^3 & \dots & u_x^n \\ 0 & l_1 & 0 & l_2 & \dots & 0 & l_n & u_y^1 & u_y^2 & u_y^3 & \dots & u_y^n \end{pmatrix} \begin{pmatrix} \delta u_x^1 \\ \delta u_y^1 \\ \delta u_x^2 \\ \delta u_y^2 \\ \vdots \\ \delta u_x^n \\ \delta u_y^n \\ \delta l_1 \\ \delta l_2 \\ \delta l_3 \\ \vdots \\ \delta l_n \end{pmatrix} \tag{3.4.3}$$

where $\delta\vec{p}^i = \delta\vec{p}(s_i,t)$, $\delta\vec{u}^i = \delta\vec{u}(s_i,t)$, $\delta\vec{l}_i = \delta\vec{l}(s_i,t)$, $\vec{l}_i = \vec{l}(s_i)$, and $\vec{u}^i = \vec{u}(s_i,t)$. The x and y components of $\delta\vec{p}(s_i,t)$ are respectively denoted δp_x^i and δp_y^i. Similary, the x,y components of $\delta\vec{u}(s_i,t)$ are δu_x^i and δu_y^i. $\delta\vec{p}$ and $\delta\vec{u}$ each have $2n$ elements, and $\delta\vec{l}$ has n elements.

For given $\delta\vec{p}$, there is not a unique solution to Eq. (3.4.3). A simplified (and unique) solution for (3.4.3) is obtained by setting $l(s_i,t) = 1\ \forall_{1\leq i\leq n}$ (i.e $\delta l(s_i,t) = 0$). Although all of the $l(s_i,t) = 1$, the snake can still use its extensibility to avoid obstacles because $\|\vec{u}^i + \delta\vec{u}^i\| \neq 1$. In other words, the length of the tangent vectors are no longer constrained to have unit length in this approximation unless additional restrictions are employed. After setting $\delta l(s_i,t) = 0$ and enforcing the end effector constraints,(3.4.3) becomes:

$$\begin{pmatrix} \delta p_x^1 \\ \delta p_y^1 \\ \delta p_x^2 \\ \delta p_y^2 \\ \vdots \\ \delta p_x^{n-2} \\ \delta p_y^{n-2} \\ 0 \\ 0 \end{pmatrix} = \begin{pmatrix} 1 & 0 & 0 & 0 & \dots & 0 & 0 & 0 & 0 \\ 0 & 1 & 0 & 0 & \dots & 0 & 0 & 0 & 0 \\ 1 & 0 & 1 & 0 & \dots & 0 & 0 & 0 & 0 \\ 0 & 1 & 0 & 1 & \dots & 0 & 0 & 0 & 0 \\ \vdots & \vdots & \vdots & \vdots & \ddots & \vdots & \vdots & \vdots & \vdots \\ 1 & 0 & 1 & 0 & \dots & 1 & 0 & 0 & 0 \\ 0 & 1 & 0 & 1 & \dots & 0 & 1 & 0 & 0 \\ 1 & 0 & 1 & 0 & \dots & 1 & 0 & 1 & 0 \\ 0 & 1 & 0 & 1 & \dots & 0 & 1 & 0 & 1 \end{pmatrix} \begin{pmatrix} \delta u_x^1 \\ \delta u_y^1 \\ \delta u_x^2 \\ \delta u_y^2 \\ \vdots \\ \delta u_x^{n-2} \\ \delta u_y^{n-2} \\ \delta u_x^{n-1} \\ \delta u_y^{n-1} \end{pmatrix} \tag{3.4.4}$$

which has a simple, obvious and easily computed solution to (3.4.4).

$$u_x^i = p_x^i - p_x^{i-1} \tag{3.4.5}$$

$$u_y^i = p_y^i - p_y^{i-1} \tag{3.4.6}$$

The discretized backbone curve is then used, via a fitting procedure, to compute the local actuator displacements which implement the desired deformation. Figure 6 displays a PSM deformation of a 30 DOF variable geometry truss manipulator (kinematically identical to the real system described in Section 4) in response to an impinging obstacle. The backbone curve is approximated by 100 segments. The manipulator is originally in a straight configuration, which locally deforms to avoid a simulated

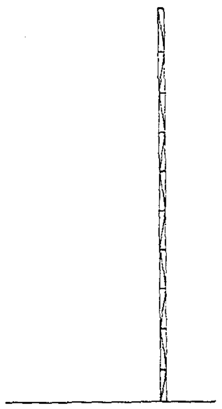
Figure 6: Original Configuration

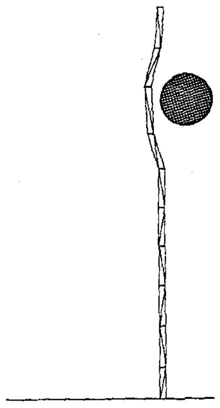
Figure 7: Resulting Configuration

obstacle in Figure 7. In this simulation, the response function is shaped like a triangle.

4. Experimental Setup

To prove the feasibility of the proposed algorithms, a distributed sensor system was developed for the 30 degree-of-freedom hyper-redundant robot system described in [ChB92b]. Figure 8 shows the structure of this testbed. This section describes the test bed structure in detail.

4.1. Hyper redundant manipulator and control system

The hyper-redundant manipulator is a modular Variable Geometry Truss design [Ch]. The 30 degree-of-freedom (DOF) planar robot consists of ten modules (also called bays) of 3 DOF each (Fig. 8). Each DOF consists of a D.C. servo motor which drives a lead screw. Each lead screw is instrumented with a linear potentiometer. The real time system controller is based on a VME-bus multiprocessing computer, currently consisting of two Heurikon (68030 and 68020) single board processors, and the VxWorks real time operating system. One processor is dedicated to the closed loop feedback control of the actuator positions. The other processor is dedicated to processing of sensor data and real time computation of the PSM algorithms.

To enable flexible, modular, and easily expandable experimentation with sensor based planning, a novel 34 wire "Sensor Bus" architecture was developed for the sensor system. One end of the sensor bus is connected to the PSM processor via a parallel port. The sensor bus consists of an eight bit outgoing data path, a four bit status line, a two bit strobe and one interrupt request line. The data path and the two strobe lines enable the CPU to access up to 256 sensors and to send eight bits of information to the sensor peripherals for possible sensor control purposes. The interrupt request line is connected to the hardware counter on the CPU board so that accurate timing measurements can be made in real time.

Sensors can be added to the system via "Sensor Interface Modules." This module decodes the sensor bus address and generates signals to control sensors. Up to two ultrasonic sensor modules and six sets of sensors which produce data with 4 bit (or less) quantization can be controlled. Currently, only four infrared sensors per board are present, though up to eight infrared sensors and eight mechanical switchs can be directly connected. The sensor interface module circuitry is mounted on a printed circuit board which is 15cm by 12cm in size. Fig. 9 shows a photograph of the sensor interface module. The sensor bus is physically connected in the bottom of the module in a daisy-chain fashion. In the figure, two ultrasonic transducers are shown above the module. Also the infrared proximity sensor is shown on the side of the module.

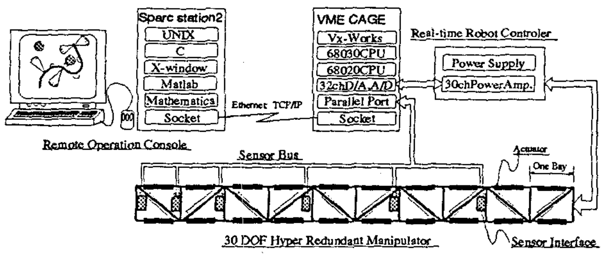

Figure 8: Hyper Redundant Robot Test Bed

4.2. Sensors

Currently, the robot has two types of sensors: infrared (IR) and ultrasonic (US). There are five sets of two US sensors. Each set is rigidly attached to alternate bays so that each sensor points outward from the backbone curve (or the centerline of the mechanism). An additional US sensor will be mounted at the front of the mechanism, pointing forward. Twenty IR sensors, again two at each the ten bays facing outward, are currently mounted on the snake. In the near future, twenty-four additional IR sensors will be added, two more at each bay, and four in front. Fig. 10 schematically shows how these sensors are distributed throughout the mechanism.

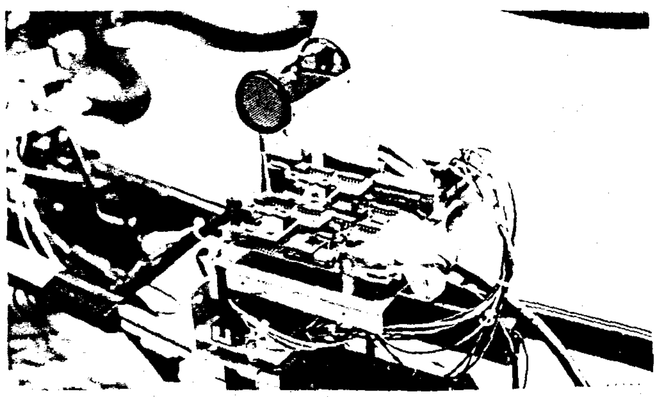
Figure 9: Sensor Interface Module

Electrostatic type ultrasonic sound transducers determine distance by measuring the time of flight of the ultrasound pulse leaving the transducer, bouncing off an object and returning to the sensor. A 50kHz sonar wave burst is transmitted when the sonar-ranging module is triggered [Ci]. The ranging module output is connected to the sensor bus interrupt request line. The echo return time is computed by the CPU hardware counter. Since the sixteen bit resolution distance measurement result is read from the hardware counter, no result is ever sent through the sensor bus. This design greatly simplifies the hardware required.

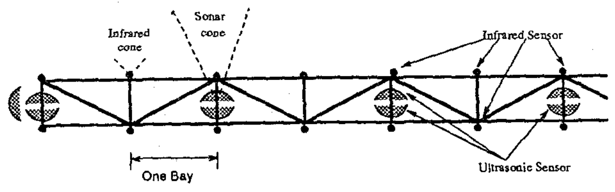

Figure 10: Sensor Arrangement

The US sensors are activated sequentially (at 16 millisecond intervals) to prevent interference between sensors. These sensors are calibrated to measure distances ranging from 10cm to 2.5m, with a 2% accuracy. There is about twenty degrees of conical ambiguity for direction, because of the transmitting beam pattern of the transducer [Ci]. In this work, it is assumed that the obstacle lies along the cone's centerline, which is locally normal to the backbone curve at the point of sensor attachment.

The IR sensors yield binary proximity information–i.e., the presence or absence of the obstacle in some pre-set range. An infrared LED emits modulated infrared light, and if an obstacle is near the robot, the IR sensor will detect the reflected light. The range of the IR system can be adjusted by setting potentiometers on the sensor boards. Currently, the IR system is set up to detect the presence of obstacles up to four inches away from the robot. Like the US, the location of an obstacle is not precisely known, but lies somewhere in a cone emanating from the IR sensor.

Each sensor has its own advantage. The IR sensors have a very fast response and can be sampled at extremely high rates. They are thus suitable for the PSM system. The US sensors provide proportional obstacle distance, rather than binary proximity information. They are thus more useful for accurate planning. However, since the US sensors are sequentially polled to prevent interference, the minimum sampling period is 176 milliseconds. The IR sensors are sequentially polled in a similar fashion, but at a significantly higher rate. To maximize the use of both types of sensors, the sensor interface module is designed to operate both US and IR sensors simultaneously in different intervals.

4.3. Remote Operation Console

The real time computers are connected to Sun workstations via the ethernet. Via software sockets, information can be transferred through the ethernet between the real time computer running VxWorks and the Sun workstations running Unix. C programs and many software packages, such as Matlab, are able to directly communicate with the real time computers via the sockets. Therefore, these programs can control the snake. The FSM and higher levels of control are implemented on the SUN workstation.

Experimental robot control programs are developed in a combination of C and Matlab. Via an X-Window interface, these programs graphically display and continually update the robot's configuration and sensor measurements. Fig.11 shows the X-Window operation console window. In addition, many motion planning and sensing commands can be executed using a graphical menu interface. End-effector via points of a hyper-redundant trajectory can be specified by a mouse, and the trajectory is then executed by the real-time system.

In addition to graphically depicting the current configuration of the manipulator, this system displays US and IR sensor measurements. The solid cones emanating from the manipulator represent US sensor data. In this representation scheme, the closet point to an obstacle in the sensor beam pattern lies somewhere on the distal arc of the cone. The dashed arcs much closer to the mechanism indicate that the IR sensors have detected nearby obstacles at these locations.

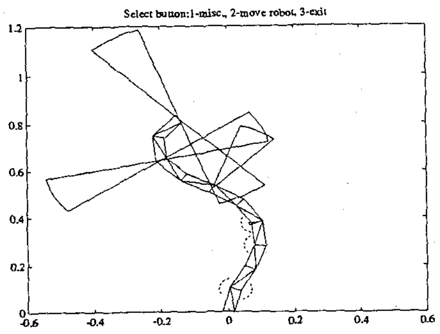

Figure 11: Operation Console

5. Results

The PSM algorithm described in Section 3.4 and the FSM algorithm of Section 3.1 have been implemented on our hyper-redundant robot test-bed. Photographs of one experiment are shown below. In this experiment, the backbone curve, dictated by some high level planner, was a straight line. The backbone curve was passed to an FSM which guaranteed that the end effector was placed at the desired location while avoiding walls and other obstacles in the laboratory. Two obstacles were moved into an unacceptably close proximity (about 10cm or 4in) to the mechanism, and the manipulator locally deformed away from each obstacle while maintaining constant end-effector position. Truthfully, the end-effector was displaced slightly from its original position (less than a 1 inch displacement over a distance of $\sim$16 feet). The current implementation of the discrete approximation algorithm employs only IR sensors, because there are many more IR sensor distributed along the snake.

This experiment showed the local shape modification capability of the PSM algorithm proposed in this paper. In real time, this PSM reliably works, especially when the actuators in the section of the robot that is deforming are not near their joint limits. As actuators limits are approached, local deformation may become infeasible. In this case, the FSM planner should be invoked to redistribute actuator displacements along the manipulator so as to move away from the joint limits. This ability is currently being implemented in our system.

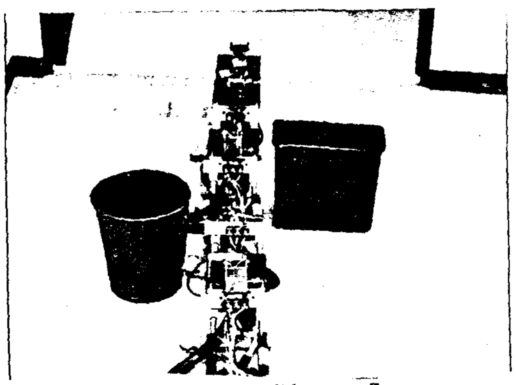
[Original Shape]

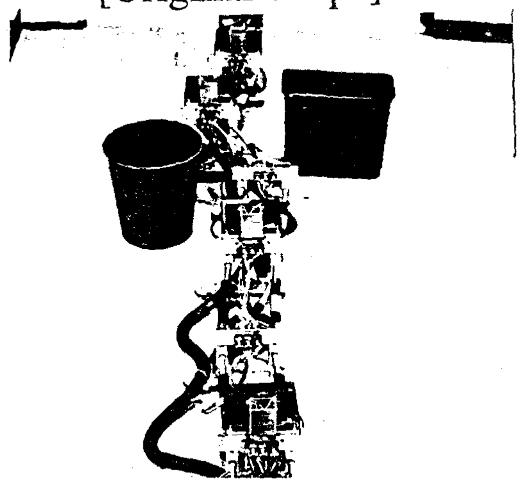
[Discrete Approximation Method]

6. Conclusion

In this paper, a local sensor based planning method for hyper-redundant robots is proposed. This method is based on a backbone curve kinematic framework and a dual-resolution decomposition of hyper-redundancy resolution into two classes of local sensor based planning methods: full shape modification (FSM) and partial shape modification (PSM). An algorithm for an FSM planner based on a null-space projection improvement in a modal space was introduced. This algorithm has a least squares characteristic for satisfying end-effector and multiple obstacle avoidance constraints. A novel "pseudo-spring" feature, which tends to return the backbone curve to its original shape, is also incorporated. However, other schemes are also possible.

These methods were implemented on an actual 30 DOF hyper-redundant manipulator test bed. An innovative sensor bus architecture and a graphical programming and display interface were reviewed. Experiments using this system showed the applicability and effectiveness of the proposed methods to real hyper-redundant manipulators. A reasonable amount of computer power was required for real-time implementation of these algorithms.

As suggested in the previous section, we are currently working to improve the FSM planner so that it can better interpret and react to exceptional conditions indicated by the PSM level. In addition, we intend to develop better sensor fuction methods which properly combine ultrasonic and infrared sensor readings from adjacent sensors. The highly distributed nature of sensors on a hyper-redundant mechanism also point to the need for new theories on deploying and using massively redundant sensor arrays. Finally, future work will focus on using sensor data for higher level hyper-redundant robotic planning.

Acknowledgements: This work has been supported by National Science Foundation Presidential Young Investigator Grant MSS-9157843, by the office of Naval Research Young Investigator Award N00014-92-J-1920, and by a grant from the NEC Corporation. The authors would like to thank Jim Ostrowski, I-Ming Chen, Tim Frank, Elon Rimon, Jim Radford, and especially Brett Slatkin for their help in constructing the sensor modules. The authors would also like to thank Dr. Tagawa and Mr. Yamamoto of the NEC Corporation for making this collaborative research opportunity possible.

7. References

[CaLi] Canny J. F., Lin, M. C. "An Opportunistic Global Path Planner," *Proc. IEEE Int. Conf. on Robotics and Automation*, Cincinnati, Ohio, May 14-17, 1990, pp. 1554-1559.

[Ch] Chirikjian, G. "Theory and Applications of *Hyper-Redundant Robotic Manipulators*," PhD Thesis, California Institute of Technology, Pasadena, Ca, 1992.

[ChB90a] Chirikjian, G.S., Burdick, J.W., "An Obstacle Avoidance Algorithm for Hyper-Redundant Manipulators," *Proc. IEEE Int. Conf. on Robotics and Automation*, Cincinnati, Ohio, May 14-17, 1990, pp. 625-631.

[ChB90b] Chirikjian, G.S., Burdick, J.W., "Kinematics of Hyper-Redundant Manipulators," *Proc. ASME Mechanisms Conference*, Chicago, IL, DE-Vol. 25, pp. 391-396, Sept. 16-19, 1990.

[ChB90c] G.S. Chirikjian and J.W. Burdick, "Applications of Hyper-Redundant Manipulators for Space Robotics and Automation," *Proc. Int. Symposium on Artificial Intelligence and Robotics Applications to Space*, Kobe, Japan, November, 1990.

[ChB91a] Chirikjian, G.S., Burdick, J.W., "Parallel Formulation of the Inverse Kinematics of Modular Hyper-Redundant Manipulators," *Proc. IEEE Int. Conf. on Robotics and Automation*, Sacramento, California, April, 1991, pp. 708-713.

[ChB91b] Chirikjian, G.S., Burdick, J.W., "Kinematics of Hyper-Redundant Locomotion with Applications to Grasping," *Proc. IEEE Int. Conf. on Robotics and Automation*, Sacramento, CA, April, 1991.

[ChB92a] Chirikjian, G.S., Burdick, J.W., "On the Determination of Kinematically Optimal Hyper-Redundant Manipulator Configurations," *Proc. IEEE Int. Conf. on Robotics and Automation*, Nice, France, May 10-15, 1992.

[ChB92b] Chirikjian, G.S., Burdick, J.W., "Design, Implementation, and Experiments with a 30 Degree-of-Freedon Hyper-Redundant Robot," *Proc. Int. Symp. Robotics and Manufacturing*, Albuquerque, NM, Nov., 1992.

[ChB92c] Chirikjian, G.S., Burdick, J.W., "A Modal Approach to Hyper-Redundant Manipulator Kinematics," submitted to *IEEE Trans. on Robotics and Automation.*

[ChB93a] Chirikjian, G.S., Burdick, J.W., "The Kinematics of Planar Hyper-Redundant Robotic Locomotion," submitted to *IEEE Trans. on Automation and Robotics.*

[ChB93b] Chirikjian, G.S., Burdick, J.W., "Curvilinear Hyper-Redundant Robotic Locomotion Over Uneven Terrain, with Applications to Grasping," submitted to *IEEE Trans. on Automation and Robotics.*

[ChB93c] Burdick, J.W., Radford, J., Chirikjian, G.S., "A 'Sidewinding' Locomotion Gait for Hyper-Redundant Robots," submitted to *IEEE Int. Conf. on Robotics and Automation*, Atlanta, GA, May, 1993.

[Ci] Ciarcia, S. "An Ultrasonic Ranging System." *Byte Magazine*, October, 1984, pp.113-123.

[HiU] Hirose, S., Umetani, Y., "Kinematic Control of Active Cord Mechanism With Tactile Sensors," *Proceedings of Second International CISM-IFT Symposium on Theory and Practice of Robots and Manipulators*, pp. 241-252, 1976.

[Gr] Greville, T.N.E. "The Pseudoinverse of a Rectangular or Singular Matrix and its Applications to the Solutions of Systems of Linear Equations," SIAM Review 1(1),1959,pp.38-43.

[Latombe] J.C. Latombe, Robot Motion Planning, Kluwer Academic Publishers, Boston, 1991.

[Li] Liegeois, A. "Automatic Supervisory Control of the Configuration and Behavior of *Multibody Mechanisms*," *IEEE Trans. Systems*, Man and Cybernetics, 1977, Vol. SMC-7, No.12, pp.868-871.

[LoWes] Lozano-Perez, T. and Wesley, M.A. "An Algorithm for Planning Collision-Free Paths Among Polyhedral Obstacles," *Communications ACM*, Oct. 1979, Vol ACM 22, pp.560-570.

[MaKl] Maciejewski, A. and Klein, C.A. "Obstacle Avoidance for Kinematically Redundant Manipulators in Dynamically Varying Environments," International Journal of Robotics Research, Vol.4, No.3, Fall, 1985, pp.109-117.

[Nak] Y. Nakamura, H. Hanafusa, and T. Yoshikawa, "Task Priority Based Redundancy Control of Robot Manipulators," *International Journal of Robotics Research*, vol. 6, 1987, pp. 3-15.

[Pe] Penrose, R. "On Best Approximate Solutions of Linear Matrix Equations," Proc. Cambridge Phill.,1956, Soc.52,pp.17-19.

[ReLu] Reznik, D. Lumelsky, V. "Motion Planning with Uncertainty for Highly Redundant Kinematic Structures I. 'Free Snake' Motion," *IEEE/RSJ International Conference on Intelligent Robots and Systems*, Raleigh, N.C., 1992.

[Sh] Sharir, "Algorithmic Motion Planning for Robots."

[Yo] Yoshikawa, T. "Analysis and control of robot manipulators with redundancy," Robotics research: The First International Symposium, ed. Brady, M. and Paul, R. Cambridge:MIT Press,1984, pp.735-747.